New parametrization of Skyrme's interaction for regularized multireference energy density functional calculations

K. Washiyama,[1,*] K. Bennaceur,[2] B. Avez,[3,4] M. Bender,[3,4] P.-H. Heenen,[1] and V. Hellemans[1]

[1]*PNTPM, Université Libre de Bruxelles, 1050 Bruxelles, Belgium*

[2]*Université de Lyon, F-69003 Lyon, France; Institut de Physique Nucléaire de Lyon, CNRS/IN2P3, Université Lyon 1, F-69622 Villeurbanne, France*

[3]*Université Bordeaux, Centre d'Etudes Nucléaires de Bordeaux Gradignan, UMR5797, F-33170 Gradignan, France*

[4]*CNRS, IN2P3, Centre d'Etudes Nucléaires de Bordeaux Gradignan, UMR5797, F-33170 Gradignan, France*

Background: Symmetry restoration and configuration mixing in the spirit of the generator coordinate method based on energy density functionals have become widely used techniques in low-energy nuclear structure physics. Recently, it has been pointed out that these techniques are ill defined for standard Skyrme functionals, and a regularization procedure has been proposed to remove the resulting spuriosities from such calculations. This procedure imposes an integer power of the density for the density-dependent terms of the functional. At present, only dated parametrizations of the Skyrme interaction fulfill this condition.

Purpose: To construct a set of parametrizations of the Skyrme energy density functional for multireference energy density functional calculations with regularization using the state-of-the-art fitting protocols.

Method: The parametrizations were adjusted to reproduce ground-state properties of a selected set of doubly magic nuclei and properties of nuclear matter. Subsequently, these parameter sets were validated against properties of spherical and deformed nuclei.

Results: Our parameter sets successfully reproduce the experimental binding energies and charge radii for a wide range of singly magic nuclei. Compared to the widely used SLy5 and to the SIII parametrization that has integer powers of the density, a significant improvement of the reproduction of the data is observed. Similarly, a good description of the deformation properties at $A \sim 80$ was obtained.

Conclusions: We have constructed new Skyrme parametrizations with integer powers of the density and validated them against a broad set of experimental data for spherical and deformed nuclei. These parametrizations are tailor-made for regularized multireference energy density functional calculations and can be used to study correlations beyond the mean field in atomic nuclei.

I. INTRODUCTION

One of the most widely used designs of an effective nucleon-nucleon interaction for mean-field-based methods [1] was introduced by Skyrme [2,3] as a combination of momentum-dependent two-body contact forces and a momentum-independent three-body contact force. The first applications [4–6] demonstrated the remarkable qualities of this interaction to describe many properties of nuclei throughout the chart of nuclei. However, some drawbacks due to an insufficient flexibility of Skyrme's original ansatz became apparent.

The early parametrizations of Skyrme's interaction led to two major problems. First, the simple contact three-body force does not allow for a realistic value of the incompressibility K_∞ of symmetric infinite nuclear matter. Typically, values of about 350 MeV were obtained, which is significantly larger than the empirical value of $210 \lesssim K_\infty \lesssim 240$ MeV [7–9]. Second, the same three-body force almost always gives rise to a spin-instability in infinite nuclear matter [10–12] and finite nuclei [13], rendering the calculation of excitations of unnatural parity in the random-phase approximation (RPA) impossible [14].

It turned out that both problems can be simultaneously solved when replacing Skyrme's three-body force $t_3 \, \delta(\mathbf{r}_1 - \mathbf{r}_2)\delta(\mathbf{r}_1 - \mathbf{r}_3)$ with a density-dependent two-body contact force $\frac{1}{6} t_3 (1 + x_3 \hat{P}_\sigma) \rho_0^\alpha [(\mathbf{r}_1 + \mathbf{r}_2)/2] \, \delta(\mathbf{r}_1 - \mathbf{r}_2)$, where $\hat{P}_\sigma$ and $\rho_0(\mathbf{r})$ are the spin-exchange operator and the isoscalar density, respectively. For $\alpha = 1$ and $x_3 = 1$, both are equivalent as long as time-reversal symmetry is conserved [4]. However, the so-called time-odd terms from the density-dependent two-body force have an isospin structure that differs from those of the three-body force, which removes the spin instability [10]. Therefore, all early parametrizations have since been used as two-body forces with a linear density dependence. In fact, the ambiguity around the three-body term was recognized from the beginning by the authors of the earliest fits of Skyrme's interaction [4,6], who pointed out that its three-body force "should not be considered as a real three-body force, but rather as convenient way of simulating the density dependence of an effective interaction" [6].

In a second step, reducing the exponent α to values between 1/6 and 1/3 allows also for a realistic compressibility [7,15,16]. The appearance of density dependencies of the form $\rho_0^\alpha(\mathbf{r})$ is also motivated through approximations to the G matrix of Brueckner-Goldstone theory [17–20]. Until now, all widely used parametrizations of the Skyrme interaction have stuck to this simple form of density dependence, although

___
*Present address: RIKEN Nishina Center, Wako 351-0198, Japan.

several extensions were attempted over time [1]. The same form of density-dependent two-body contact force is also used to complement the finite-range Gogny interaction [21,22]. Modifications of specific terms in the total energy have been made as well, hence, abandoning the link to an underlying force [1]. It is then more appropriate to refer to a Skyrme energy density functional (EDF).

There have been many adjustments of the parameters of Skyrme's interaction since the 1970s [1]. The range of data on which the parameters are fitted has been varied and extended, sometimes with choices dictated by specific applications. Most fitting protocols, however, are designed to deliver multipurpose parametrizations that can be used for applications as diverse as the description of ground-state masses and density distributions, deformations, and rotational bands, the response to external probes, fission, and reaction dynamics for nuclei all over the mass table, and even the properties of neutron stars. One of these is the protocol by Chabanat *et al.* developed in the 1990s [23,24], which led to a significant improvement of isospin properties by including pseudodata for neutron matter. The resulting parametrizations, in particular SLy4, have been extensively tested and used for the description of many properties of atomic nuclei throughout the nuclear chart.

The Skyrme interaction was designed for use in self-consistent methods, i.e., Hartree-Fock (HF), HF + BCS, Hartree-Fock-Bogoliubov (HFB), in both their static and time-dependent variants, and in RPA. From the 1990s, Skyrme's interaction was also frequently employed in extensions of mean-field methods, such as the construction of a microscopic Bohr Hamiltonian [25,26], exact projection [27,28], and configuration mixing by use of the generator coordinate method (GCM) [29–34]. Two issues were apparent from the beginning, one related to the adjustment of the parameters of the interaction and the other to its analytical form.

Because the adjustment of the parameters is done within the mean-field approximation, the inclusion of beyond-mean-field correlations will often give rise to an overbinding of nuclei, in particular of those used during the fit. The extra binding, however, was always found to be within a few MeV and appears to saturate quickly when several collective modes and symmetry restorations are added consecutively [34]. Here, we shall not consider this issue as overbinding constitutes a small smooth trend that at the present stage is smaller than other systematic errors and/or uncertainties [1,29,35–37]. Instead, we will postpone the role of correlations on the outcome of a parameter fit to future work and concentrate on the setup of the functional itself.

As already mentioned, the Skyrme functional is adopted in extensions of the mean-field approach. Such a functional is *a priori* defined only for mean-field calculations, i.e., for a single mean-field wave function, whereas beyond-mean-field calculations require determination of a matrix element between wave functions generated by two different mean fields. Unlike a formalism based on a Hamiltonian, the extension of a density functional from a single-reference (SR) definition to a multireference (MR) one is not an unambiguous procedure. In the early applications of GCM using a Skyrme functional [30], the SIII and SIV parametrizations were indeed used as two- and

three-body forces to calculate matrix elements between two different mean-field wave functions. Taking advantage of the generalized Wick theorem derived by Balian and Brézin [38], this amounts to replacing the mean-field densities that enter the energy density by so-called *mixed densities*. This scheme for the construction of the energy density was also followed in Ref. [31], where the parametrization SIII was adopted as a density-dependent energy functional to construct the energy kernel in a GCM calculation mixing mean-field states with different axial quadrupole deformation. This procedure was not altered until very recently in subsequent applications with more recent functionals of the Skyrme, Gogny, and relativistic type [29,34,39,40] that often include multiple symmetry restorations.

However, such a generalization of the functional ignores several complications, in particular the fact that the mixed densities can become complex in MR calculations and that, often, different functionals are chosen in the mean-field and pairing channels. Still, the substitution of mean-field densities by mixed densities in the construction of the MR EDF was used with some success in many applications, despite its drawbacks that can, in principle, lead to unreliable results for an energy functional. In one way or the other, the problems of the functionals mentioned thus far are related to the breaking of the Pauli principle [41–43]. In the standard Skyrme EDF, this has many facets. First, the density dependence itself cannot be written in a completely antisymmetrized form. Second, it is customary to use different effective interactions for the particle-hole and particle-particle parts of the EDF. In addition, certain exchange terms of the Skyrme interaction are sometimes neglected or modified, and, for the Coulomb exchange term, approximations are used. All of these are either motivated by phenomenology or by computational reasons. For an overview, we refer to Ref. [1]. The standard density dependence $\rho_0^\alpha(\mathbf{r})$ poses one additional problem. In all currently used prescriptions, the density entering the density dependence might become complex. For noninteger values of α, the function $\rho_0^\alpha(\mathbf{r})$ then becomes a nonanalytical function of ρ_0 that is multivalued and exhibits branch cuts [41,42,44]. To resolve this particular issue, some alternatives for the density dependence were formulated. Indeed, several studies have concentrated on the most appropriate definition of the density dependence in MR calculations, primarily for symmetry restorations [39,42,45–48]. The question, however, is not settled yet.

The net result of these problems is that the off-diagonal terms in the MR EDF can exhibit discontinuities or even divergences when varying one of the collective coordinates. We refer to Refs. [41–44,49] for an in-depth analysis of these issues but present the arguments for the lack of signs of their presence in the published GCM calculations. First, the problems are especially critical for very light nuclei, but applications were often devoted to medium-mass and heavy ones. Second, the discretizations commonly chosen for numerical reasons when setting up projection and GCM restrain the contamination of the energy with nonphysical contributions to a very small scale.

One possibility to avoid these problems altogether would be a return to a Skyrme-force-based Hamiltonian. This, however,

will inevitably demand the systematic addition of higher-order terms in the Skyrme force, as within the standard form it is impossible to construct a parametrization that, at the same time, describes the empirical properties of nuclear matter, has no spin or other instabilities, and gives attractive pairing. By contrast, within an energy functional framework a fair description of nuclear matter and finite nuclei is achieved within the standard form. Thus, to keep the effective interaction simple, it appears to be preferable to work with a functional instead of a force. To enable their use in a MR framework, tools to by-pass the obstacles outlined above by a regularization of the Skyrme functional have been designed recently [43,49]. They require, however, that the functional dependence on the density has an integer power [44].

In this article, we construct Skyrme functionals that have the same density dependence as SIII and thereby are regularizable in the sense of Ref. [43]. The first parametrizations of the Skyrme functional built about 40 years ago [6] had all these properties, but, since then, the fitting protocols have significantly evolved and these early parametrizations certainly have to be reconsidered. Our study is based on the protocol first used for the SLyx parametrizations [23,24] that has proven to be efficient to construct functionals used successfully in a large number of applications. In this first study, we will restrict ourselves to the standard form of the Skyrme functional. The construction of a regularizable functional including higher-order density-dependent terms is underway [50,51] and will be reported elsewhere. However, we take the opportunity of the present study to include a new set of data in the fitting protocol, which are used to validate (or reject) the parametrizations.

There is a major conceptual difference between the parametrization of the Skyrme functional that we aim at and the ones by Kortelainen *et al.* [52,53], who have recently adjusted new Skyrme parametrizations on a large set of data. The aim of Kortelainen *et al.* is to describe the nucleus in the spirit of the density functional theory [54] that is very successful in condensed matter physics. Staying on the computationally simple single-reference level, as much correlation energy as possible is incorporated into the energy functional. Our aim is to construct a parametrization of the Skyrme EDF that will be used in beyond-mean-field calculations, i.e., where specific correlations are to be calculated explicitly in a multireference framework. Both views are complementary. The advantage of our approach is that it enables us to calculate spectra and transition probabilities directly in the laboratory frame of reference and avoids the ambiguities related to approximate determinations of spectroscopic quantities, whereas its disadvantage is that, even for standard observables, high predictive power will require the time-consuming calculation of correlations beyond the mean field. In the following, we will call the method that we have already used in many applications and where mean-field wave functions generated by a constraint on a collective variable are projected on particle numbers and angular momentum and mixed by the GCM the "beyond mean-field method."

The article is organized as follows. Section II reviews the fitting protocol used here and its differences to the one used to construct the SLyx parametrizations in the past. In Sec. III,

we will test the parametrizations on a large set of typical observables for spherical and deformed nuclei, including masses, separation energies, charge radii, deformations, the fission barrier of ^{240}Pu, and the moment of inertia of a superdeformed rotational band in ^{194}Hg. Section IV will summarize our findings.

II. FITTING PROTOCOL

A. The energy functional

The standard density-dependent Skyrme interaction has the form [35]

$$v(\mathbf{R}, \mathbf{r}) = t_0 \left(1 + x_0 \hat{P}_\sigma\right) \delta(\mathbf{r}) + \tfrac{1}{6} t_3 \left(1 + x_3 \hat{P}_\sigma\right) \rho_0^\alpha(\mathbf{R}) \, \delta(\mathbf{r})$$
$$+ \tfrac{1}{2} t_1 \left(1 + x_1 \hat{P}_\sigma\right)[\hat{\mathbf{k}}'^2 \, \delta(\mathbf{r}) + \delta(\mathbf{r}) \, \hat{\mathbf{k}}^2]$$
$$+ t_2 \left(1 + x_2 \hat{P}_\sigma\right) \hat{\mathbf{k}}' \cdot \delta(\mathbf{r}) \, \hat{\mathbf{k}}$$
$$+ i \, W_0 \left(\hat{\boldsymbol{\sigma}}_1 + \hat{\boldsymbol{\sigma}}_2\right) \cdot \hat{\mathbf{k}}' \times \delta(\mathbf{r}) \, \hat{\mathbf{k}}, \qquad (1)$$

where we use the shorthand notation $\mathbf{r} \equiv \mathbf{r}_1 - \mathbf{r}_2$ and $\mathbf{R} \equiv \tfrac{1}{2}(\mathbf{r}_1 + \mathbf{r}_2)$ for the relative distance and center-of-mass coordinates, respectively, where $\hat{P}_\sigma$ is the spin exchange operator, $\hat{\mathbf{k}} \equiv -\tfrac{i}{2}(\boldsymbol{\nabla}_1 - \boldsymbol{\nabla}_2)$ the relative momentum operator acting to the right, $\hat{\mathbf{k}}'$ is the complex conjugate of $\hat{\mathbf{k}}$ acting to the left, and $\rho_0(\mathbf{R})$ is the isoscalar density. The Skyrme interaction (1) contains in total 10 parameters t_0, t_1, t_2, t_3, x_0, x_1, x_2, x_3, W_0, and α to be adjusted to data.

As it is customary, we only calculate the particle-hole part of the EDF from Eq. (1). We keep, however, all terms in that channel, which is not always done [1]. For the special case of time-reversal invariance and spherical symmetry, this leads to

$$\mathcal{E}_{\text{Skyrme}} = \int d^3r \sum_{t=0,1} \left\{ C_t^\rho[\rho_0]\rho_t^2 + C_t^{\Delta\rho} \rho_t \Delta\rho_t \right.$$
$$\left. + C_t^\tau \rho_t \tau_t + \tfrac{1}{2}C_t^J \boldsymbol{J}_t^2 + C_t^{\nabla \cdot J} \rho_t \nabla \cdot \boldsymbol{J}_t \right\}, \qquad (2)$$

where ρ, τ, and $\boldsymbol{J}$ are the density, kinetic density, and spin-current vector density, respectively, and the index t labels isoscalar ($t = 0$) and isovector ($t = 1$) densities. The definition of these densities and the relations between the coefficients C_t in Eq. (2) and the parameters in Eq. (1) can be found in Ref. [35]. Note that the coefficients $C_t^\rho[\rho_0]$ depend on the isoscalar density $\rho_0(\boldsymbol{r})$, whereas all others are just numbers. In case of deformed nuclei and when breaking intrinsic time-reversal symmetry, there are additional terms in the Skyrme EDF for which we refer to Refs. [35,55]

The total energy is given by the sum of the Skyrme EDF (2), the Coulomb energy, the kinetic energy, the center-of-mass correction, and the pairing energy. As in our previous studies, we have chosen a density-dependent zero-range pairing interaction [1,55,56], which leads to a functional of the form

$$\mathcal{E}_{\text{pairing}} = \frac{V_0}{4} \sum_{q=p,n} \int d^3r \left[1 - \frac{\rho_0(\mathbf{r})}{\rho_c}\right] \tilde{\rho}_q(\mathbf{r}) \, \tilde{\rho}_q^*(\mathbf{r}). \qquad (3)$$

The switching density $\rho_c = 0.16$ fm^{-3} is set to the empirical nuclear saturation density, such that the pairing interaction is most active on the surface of the nucleus. The pairing functional depends on the local pair density $\tilde{\rho}_q(\mathbf{r})$ [55] of

protons and neutrons, labeled by $q = p, n$, and the isoscalar local density $\rho_0(\mathbf{r})$. An energy cutoff of 5 MeV in the single-particle spectrum is taken above and below the Fermi energy [57]. The strength V_0 will be adjusted separately for each parametrization of the Skyrme interaction.

For most (if not all) Skyrme interactions constructed up to now, the Coulomb exchange energy has been replaced by its Slater approximation [1] that amounts to a local energy density of the form $\sim \rho_p^{4/3}(\mathbf{r})$, i.e., a term depending on a noninteger power of the density. Like the standard density dependence in the Skyrme EDF $\sim \rho_0^\alpha(\mathbf{r})$ with $0 < \alpha < 1$, this term cannot be regularized with the currently available techniques [44]. For interactions that can be safely used in regularized MR EDF calculations, the Coulomb exchange energy has to be either treated exactly or to be omitted. For simplicity, we have chosen to neglect it in the mean-field channel in the present study since an exact treatment of the Coulomb exchange field makes all calculations much more time-consuming. In addition, phenomenological arguments have also been brought forward that justify this course of action [58–60]. As usually done, the contribution of the Coulomb interaction to the pairing channel is neglected.

For the center-of-mass correction, we employ the widely used approximation where only the one-body term is considered [61]. However, the often neglected $\mathbf{J}^2$ term in the Skyrme functional (2) is kept. The latter two choices correspond to the ones made for the parametrization SLy5 of Chabanat *et al.* [24].

B. The protocol

The first step of our fitting protocol is similar to the one used for the construction of the SLyx parametrizations [23,24]. During this step, we minimize a merit function, which is a weighted sum of squared residuals,

$$\chi^2 = \sum_A \chi_A^2, \quad \chi_A^2 = \frac{1}{N_A} \sum_{i=1}^{N_A} \left(\frac{O_i - O_i^{\text{calc.}}}{\Delta O_i} \right)^2. \quad (4)$$

The O_i are experimental data for finite nuclei and empirical values for nuclear matter and the ΔO_i are tolerance parameters used to weight these data during the fit. Five categories of data are used: (i) nuclear matter properties around the saturation point, (ii) neutron matter equation of state, (iii) binding energies of doubly-magic nuclei, (iv) charge radii, and (v) spin-orbit splittings of neutron and proton states.

The nuclear matter properties that we have included are as follows:

(i) the saturation density $\rho_{\text{sat}} = 0.16 \, \text{fm}^{-3}$ with a tolerance $\Delta O_i = 0.003 \, \text{fm}^{-3}$;
(ii) the binding energy per nucleon $E/A = -16 \, \text{MeV}$ with $\Delta O_i = 0.3 \, \text{MeV}$;
(iii) the symmetry energy $a_{\text{sym}} = 31 \, \text{MeV}$ with $\Delta O_i = 1 \, \text{MeV}$; and
(iv) the Thomas-Reiche-Kuhn sum-rule enhancement factor $\kappa_v = 0.25$ with $\Delta O_i = 0.15$.

Since the incompressibility of nuclear matter K_∞ cannot be adjusted to a realistic value with the restriction imposed

on $\alpha = 1$ [23], this quantity is not considered in our fitting protocol.

The binding energies of six doubly magic nuclei are included: ^{48}Ca, ^{132}Sn, and ^{208}Pb with tolerances of $\Delta O_i = 0.2 \, \text{MeV}$; ^{40}Ca and ^{100}Sn with $\Delta O_i = 0.5 \, \text{MeV}$; and ^{56}Ni with $\Delta O_i = 0.75 \, \text{MeV}$. We allow for larger ΔO_i for $N = Z$ nuclei as one always has difficulties to reproduce their binding energy at the mean-field level. However, the discrepancies cannot be simply related to the Wigner energy that cannot be described by mean-field calculations. Usually only ^{56}Ni turns out to be underbound, whereas ^{40}Ca and ^{100}Sn are overbound. The charge radii of ^{40,48}Ca, ^{56}Ni, ^{132}Sn, ^{208}Pb have a tolerance $\Delta O_i = 0.02 \, \text{fm}$, and the spin-orbit splittings of the neutron $3p$ levels and the proton $1h$ levels in ^{208}Pb both have a tolerance $\Delta O_i = 0.2 \, \text{MeV}$.

For the neutron matter equation of state, O_i are the energies per neutron for $\rho \leqslant 0.5 \, \text{fm}^{-3}$ predicted by Wiringa *et al.* [62] with the bare two-body UV14 potential and three-body UVII potential. The tolerance parameters are set to $\Delta O_i = 0.2 \times O_i$.

These data are used to determine a first set of values of the Skyrme parametrization. The resulting EDF is then tested on several properties of finite nuclei that will be discussed in the following sections. Among these properties, the charge radii were strongly underestimated with the first set of weights that we have used. Therefore, we have chosen to relax the weights of nuclear matter properties, especially, the density at saturation and the constraints on neutron matter properties. After some attempts, this was sufficient to arrive to a satisfactory reproduction of charge radii. The weights that are given above are the final weights used in the fit.

During the first attempts to fit our new parametrizations, we encountered finite-size isospin instabilities that are characterized by a separation of protons and neutrons as examined in Ref. [63]. The instability appears when the coupling constant $C_1^{\Delta\rho} = \frac{3}{32}t_1(\frac{1}{2} + x_1) + \frac{1}{32}t_2(\frac{1}{2} + x_2)$ in the Skyrme EDF (2) takes too large a value. To prevent such instabilities, we enforce a condition on the coupling constant,

$$\chi_A^2 = \begin{cases} \left(\frac{C_{1,\text{calc}}^{\Delta\rho} - C_{1,\text{max}}^{\Delta\rho}}{1.5} \right)^2 & \text{for} \quad C_{1,\text{calc}}^{\Delta\rho} \geqslant C_{1,\text{max}}^{\Delta\rho}, \\ 0 & \text{for} \quad C_{1,\text{calc}}^{\Delta\rho} < C_{1,\text{max}}^{\Delta\rho}, \end{cases} \quad (5)$$

where the empirical choice for the maximum value $C_{1,\text{max}}^{\Delta\rho} = 25 \, \text{MeV} \, \text{fm}^5$ has been found to lie safely within the stable zone. We have also checked that the parametrizations do not lead to finite-size instabilities due to the $\mathbf{s}_t \cdot \Delta\mathbf{s}_t$ terms in the time-odd part of the Skyrme EDF [55] when setting the corresponding coupling constants to their Skyrme force value.

III. RESULTS

A. New parameter sets

The fact that we do not constrain the compressibility of nuclear matter leaves some freedom in the choice of the effective mass, cf. the discussion in Ref. [23]. We have constructed four parameter sets corresponding to values of the isoscalar effective mass m_0^* from 0.7 to 1.0 times the nucleon

TABLE I. New parameter sets for the Skyrme energy functional with effective masses as indicated.

	0.7	0.8	0.9	1.0
t_0 (MeV fm^3)	-1122.408	-1100.272	-1082.609	-1066.976
t_1 (MeV fm^5)	440.572	359.568	295.999	245.431
t_2 (MeV fm^5)	-197.528	-210.840	-240.653	-245.314
t_3 (MeV fm^6)	11 906.299	13 653.845	15 003.161	16 026.086
x_0	0.394 119	0.445 280	0.491 775	0.525 497
x_1	0.068 384	0.224 693	0.389 884	0.603 399
x_2	$-0.752 728$	$-0.615 015$	$-0.579 284$	$-0.500 115$
x_3	0.946 945	0.639 947	0.512 106	0.366 056
W_0(MeV fm^5)	119.125	110.828	103.516	97.977
α	1	1	1	1

mass m. We will refer to these as SLyIII.xx, where xx is the value of m_0^*/m.

The coupling constants of these four parametrizations are listed in Table I and the corresponding saturation properties of infinite homogeneous nuclear matter in Table II. As expected, the value of K_∞ is much too large. It increases with the effective mass [23] and there is no room to obtain a value close to the empirical value when imposing $\alpha = 1$ without introducing additional terms in the Skyrme functional. To obtain a reasonable agreement between theory and experiment for charge radii requires relaxation of the constraint on $\rho_{\rm sat}$, leading to a value lower than the usual one of 0.160 fm^{-3} but still larger than the one for SIII.

The equation of state E/A of symmetric infinite matter obtained with SLyIII.0.8 is compared with results for SLy5 and SIII in Fig. 1. As can be expected from the values for K_∞, it is stiffer than the equation of state obtained with SLy5.

In the same figure, we also compare the binding energy per neutron for pure neutron matter determined using SLy5, SIII, and SLyIII.0.8 to *ab initio* results obtained by Wiringa *et al.* [62]. On the scale of the plot, obvious differences between the parametrizations appear only at rather large densities $\rho_n \gtrsim$ 0.12 fm^{-3}. At values below, the results obtained with the three parametrizations cannot be easily distinguished, in spite of the fact that SIII was not fitted to this quantity. For larger densities, however, as expected, the inclusion of the neutron matter equation of state in the fitting protocol improves the results obtained with SLyIII.xx with respect to those of SIII. For SLy5, the tolerance in the merit function [Eq. (4)] has been chosen to be much smaller than for the SLyIII.xx, leading to a better reproduction of the equation of state.

The residuals of binding energies and charge radii of doubly magic nuclei are displayed in Fig. 2 and the corresponding values of χ^2 are given in Table III. In both cases, the new parametrizations perform much better than SIII and SLy5, irrespective of the value of the effective mass. We have to recall, however, that SIII and SLy5 were fitted with different protocols, such that the comparison of the χ^2 can serve only as a guideline for the relative performance of the parametrizations for these specific observables. It does not allow us to judge their overall quality. In particular, as discussed above, SLy5 gives a much better description of some key nuclear matter properties that cannot be adjusted with SLyIII.xx.

1. Adjustment of the pairing strength

To compute spherical and deformed open-shell nuclei, pairing correlations need to be taken into account. The functional form and the adjustment of a pairing interaction is a problem that requires, in principle, a dedicated study of its own [67,68]. Since our focus is on the properties of the interaction used in the particle-hole channel, we restrict ourselves to the surface pairing energy density functional (2) that we have used in numerous past studies.

The pairing strength V_0 in Eq. (2) is fitted in ^{120}Sn on the neutron spectral pairing gap $-\mathcal{E}_{{\rm pairing},n}/\int d^3r \; \tilde{\rho}_n(\mathbf{r})$ [67,68]. In this expression, $\mathcal{E}_{{\rm pairing},n}$ is the pairing energy of the neutrons and $\tilde{\rho}_n(\mathbf{r})$ the neutron pair density, respectively. The empirical value is determined by a five-point formula for the gap [67] and is equal to 1.393 MeV. The pairing strengths obtained for the four values of the effective mass are listed in Table IV. They are very close to each other and do not scale significantly with the effective mass.

TABLE II. Saturation properties of nuclear matter as obtained with the new parameter sets. Values for SIII and SLy5 are shown for comparison.

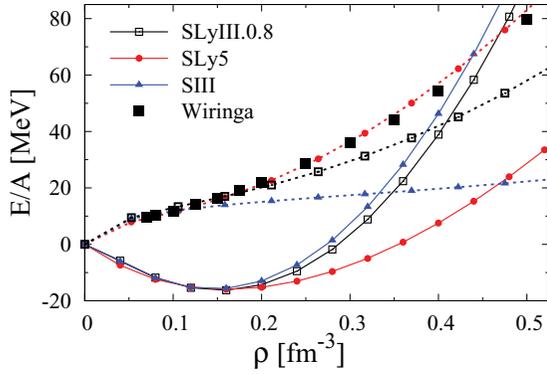|	0.7	0.8	0.9	1.0	SIII	SLy5
$\rho_{\rm sat}$ (fm^{-3})	0.153	0.153	0.153	0.153	0.145	0.160
E/A (MeV)	-16.33	-16.32	-16.31	-16.31	-15.85	-15.98
m_0^*/m	0.700	0.800	0.900	1.000	0.763	0.697
K_∞ (MeV)	361.3	368.7	374.5	379.4	355.4	229.9
$a_{\rm sym}$ (MeV)	31.98	31.69	31.44	31.31	28.16	32.03
κ_v	0.612	0.467	0.336	0.250	0.525	0.250

FIG. 1. (Color online) Binding energy per nucleon E/A for symmetric nuclear matter (solid lines) and for pure neutron matter (dotted lines) as a function of nucleon density ρ. The solid squares indicate empirical values of the neutron matter equation of state by Wiringa *et al.* [62].

B. Spherical nuclei

We start our validation of the SLyIII.xx interactions by confronting their predictions with various experimental data for singly magic nuclei.

1. Binding energies

The differences between the calculated and the experimental binding energies are shown in Figs. 3 and 4 for representative isotopic and isotonic chains of singly magic nuclei. The agreement with the data is in general better for the SLyIII.xx parametrizations than for SIII and SLy5. To quantify these energy differences, we have defined two mean deviations,

$$E_{\mathrm{dev}} = \frac{1}{N}\sum_{i=1}^{N}\left|E_i - E_i^{\mathrm{expt.}}\right|, \qquad (6)$$

$$E_{\mathrm{rel}} = \frac{1}{N}\sum_{i=1}^{N}\frac{\left|E_i - E_i^{\mathrm{expt.}}\right|}{\left|E_i^{\mathrm{expt.}}\right|}, \qquad (7)$$

where N is the total number of singly magic nuclei that have been calculated. Analogous quantities can be defined
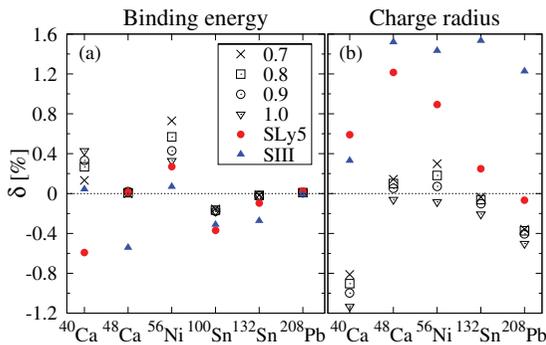
FIG. 2. (Color online) Residuals between calculated and experimental values [64–66], defined as $\delta = (O^{\mathrm{calc.}} - O^{\mathrm{expt.}})/|O^{\mathrm{expt.}}|$, for binding energies and charge radii of doubly magic nuclei.

TABLE III. χ^2 values in Eq. (4) for binding energies E and charge radii r_c.

	0.7	0.8	0.9	1.0	SIII	SLy5
E	5.12	4.33	3.93	4.02	63.99	14.80
r_c	0.67	0.74	0.87	1.22	7.79	1.74

for charge radii. The values given in Table V confirm that the agreement with data is improved by the SLyIII.xx parametrizations. Deviations for binding energies E_{dev} decrease with increasing effective mass.

Let us recall that our aim is to construct an interaction well suited for adding the correlations generated by symmetry restorations and configuration mixing calculations. Therefore, the nuclei calculated at the mean-field level of approximation should be underbound and in such a manner that the difference between mean-field calculation and data is slightly larger for midshell nuclei than for doubly magic ones [29].

It is clear that the SLyIII.xx parametrizations with the largest values of m_0^*/m leave nearly no room for the addition of correlation energies in the Sn and Pb chains. The increase of the effective mass washes out the shell effects in the mean-field results. At this point, SLyIII $m_0^*/m = 0.8$ is the most promising parametrization, underbinding the energy of the Sn and Pb isotopes by what can be expected to be added from correlations.

2. Charge radii

The calculated and experimental charge radii are compared in Fig. 5. The charge radii are determined according to Ref. [23], taking into account the internal charge distribution of both protons and neutrons and adding a correction for the electromagnetic spin-orbit effect. The corresponding deviations, defined in Eqs. (6) and (7), are given in Table V. The SLyIII.xx parametrizations clearly provide a better description of these data than SIII, which systematically underestimates the charge radii. SLy5, on the other hand, leads to even larger radii and, therefore, performs in general better than the SLyIII.xx. As can be seen from Table V, the deviations from the data R_{dev} and R_{rel} decrease with decreasing effective mass.

Again, we recall that correlations from fluctuations in the quadrupole degree of freedom consistently increase the charge radii of spherical nuclei [29]. Overall, the observed trend of the charge radii is well reproduced by the calculation. The deviations from the smooth trend observed in the data for the Pb and Ca isotopes and for the $N = 82$, and 126 isotones are not described by any of the parametrizations and seemingly require either the inclusion of explicit correlations or higher-order terms in the EDF, cf. Ref. [1] and references therein.

TABLE IV. Pairing strength V_0 for the parametrizations as indicated. The switching density is set to 0.16 fm^{-3} in all cases.

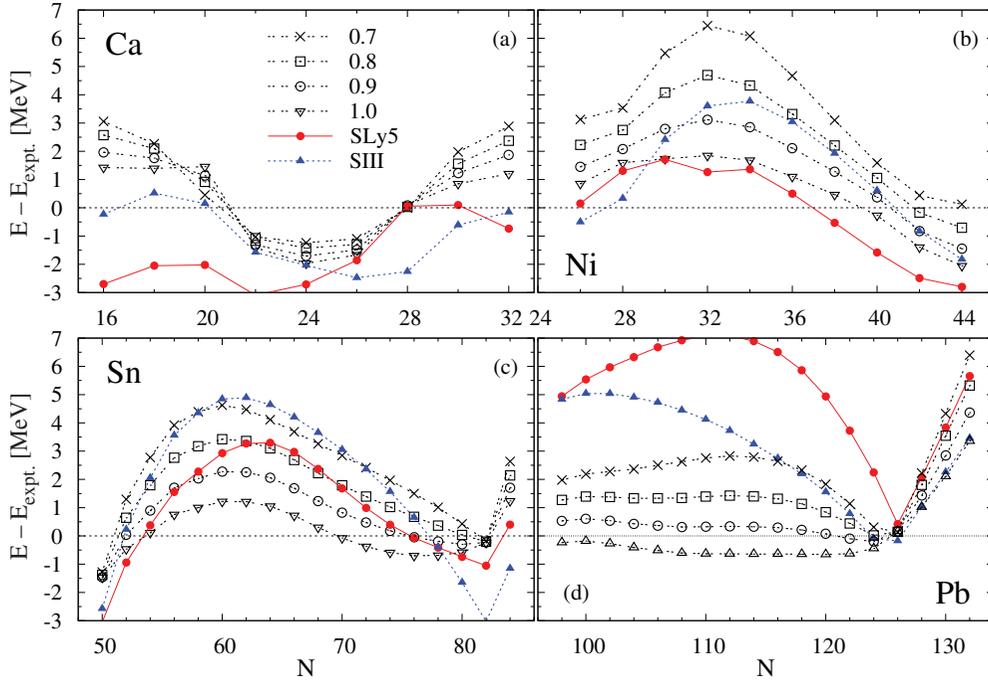|	0.7	0.8	0.9	1.0	SLy5	SIII
V_0 (MeV fm^3)	−994	−987	−985	−988	−977	−944

FIG. 3. (Color online) Residuals of the binding energy $E - E_{\text{expt.}}$ as a function of neutron number N for the Ca, Sn, Ni, and Pb isotopic chains obtained with the parametrizations as indicated. Experimental data are taken from Ref. [64].

3. Two-neutron separation energies

The two-neutron separation energies are compared to the experimental data in Fig. 6 for the Ca, Ni, Sn, and Pb isotopic chains. All six parametrizations give similar results for midshell nuclei. They tend to overestimate the characteristic

jump at neutron magic numbers, which, however, would be reduced by dynamical quadrupole correlations [29]. For Ca and Ni isotopes, our values do not reproduce the slope of the experimental data for midshell nuclei. For the Sn and Pb isotopes, the agreement with the data is improved by SLyIII.xx with respect to SIII and SLy5.
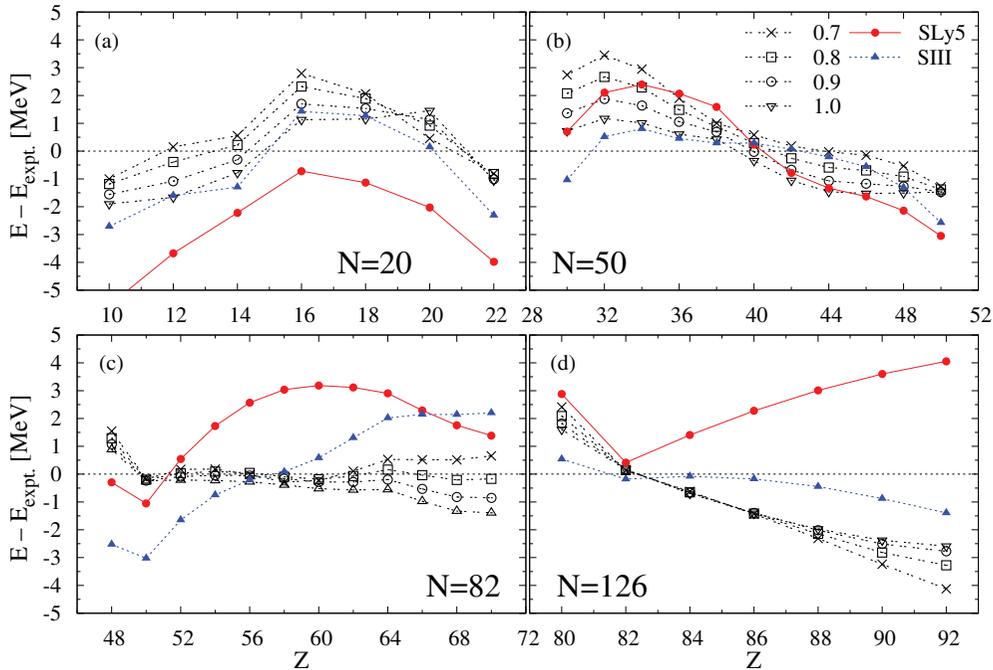
FIG. 4. (Color online) Same as in Fig. 3 but for $N = 20, 50, 82, 126$ isotonic chains as a function of proton number Z.

TABLE V. Mean deviation with respect to the data for binding energies and charge radii obtained for the parametrizations as indicated.

	E_{dev} (MeV)	E_{rel} (%)	r_{dev}^c (fm)	r_{rel}^c (%)
SLyIII.0.7	1.97	0.26	0.018	0.40
SLyIII.0.8	1.46	0.21	0.020	0.46
SLyIII.0.9	1.09	0.17	0.023	0.52
SLyIII.1.0	0.98	0.15	0.029	0.65
SLy5	2.49	0.31	0.012	0.29
SIII	1.88	0.23	0.051	1.09

4. Single-particle energies

Until now, our analysis of the Skyrme parametrizations has been limited to data for which the comparison between theory and experiment is model independent. This is no longer the case for single-particle energies, for which there exist several conflicting definitions that often even do not correspond to observables [70]. Here, we use the eigenvalues of the single-particle Hamiltonian. They provide a lowest-order approximation to separation energies, which should be corrected for polarization effects [1] and the coupling to vibrations, cf. Refs. [71,72]. In Fig. 7, single-particle energies
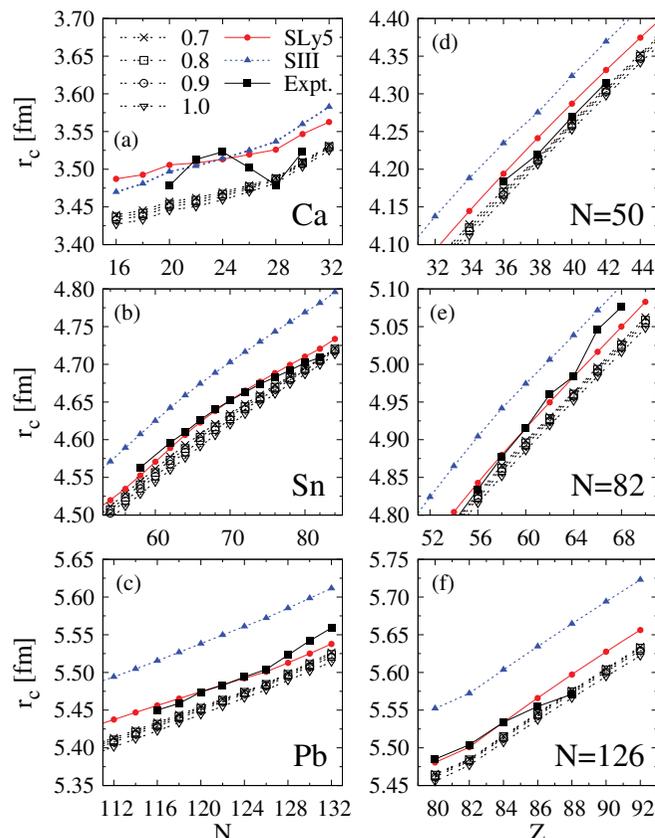
FIG. 5. (Color online) Charge radii for Ca, Sn, Pb isotopic chains and for $N = 50, 82, 126$ isotonic chains obtained by SLyIII, SLy5, and SIII. Experimental data shown by solid squares are taken from Ref. [69].
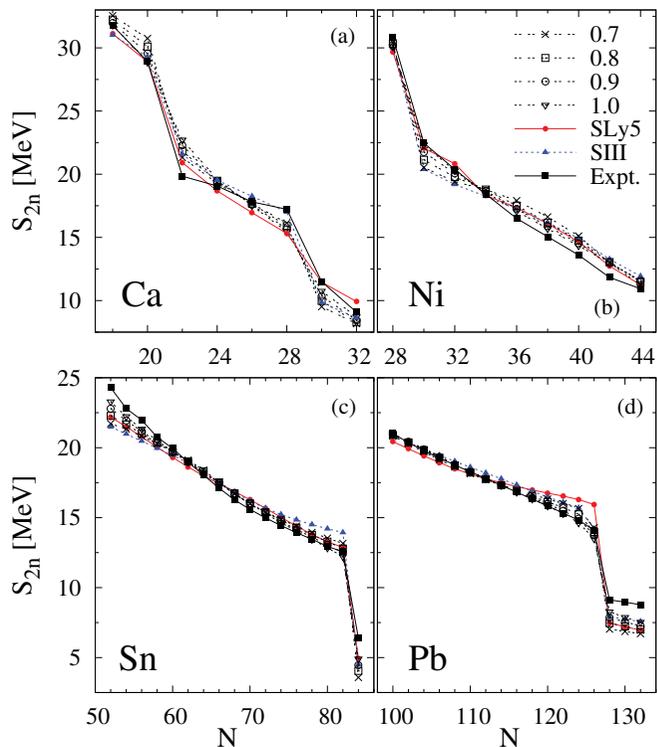
FIG. 6. (Color online) Two-neutron separation energies for Ca, Ni, Sn, and Pb isotopes calculated with the parametrizations as indicated.

are compared to one-nucleon separation energies to or from doubly magic nuclei.

For ^{40}Ca and ^{132}Sn, the spectra obtained with the SLyIII.xx parametrizations are very similar to those of SIII. For ^{208}Pb, there are several differences, in particular concerning the position of high-j levels.

A rule of thumb predicts that a higher effective mass gives a more compressed spectrum. We are in a good position to check this rule. The SLyIII.xx have been constructed using exactly the same protocol but correspond to four values of the effective mass. They are a modern version of SIII but share with it many similarities. Looking to Fig. 7, a higher effective mass corresponds indeed to a more compressed spectrum. However, a change in the effective mass does not correspond to a simple rescaling of the single-particle spectra. For neutron holes in ^{208}Pb or neutron particles in ^{132}Sn, the relative distances between levels hardly vary at all. Also, this rule of thumb is no longer valid for a change in the fitting protocol, as exemplified by SIII. The differences between the single-particle spectra obtained with SIII and the SLyIII.xx cannot be due to the effective mass. The SLy5 results sometimes differ markedly. In all cases, the reproduction of the experimental gaps is rather poor. A more detailed analysis would require direct computation of one-nucleon separation energies, including correlations beyond the mean field which are known to give a sizable contribution to the two-nucleon separation energies to and from doubly magic nuclei [29,73]. We present below, in Sec. III C4, results for self-consistent calculation of binding energies of a few very heavy odd-A well-deformed nuclei, for
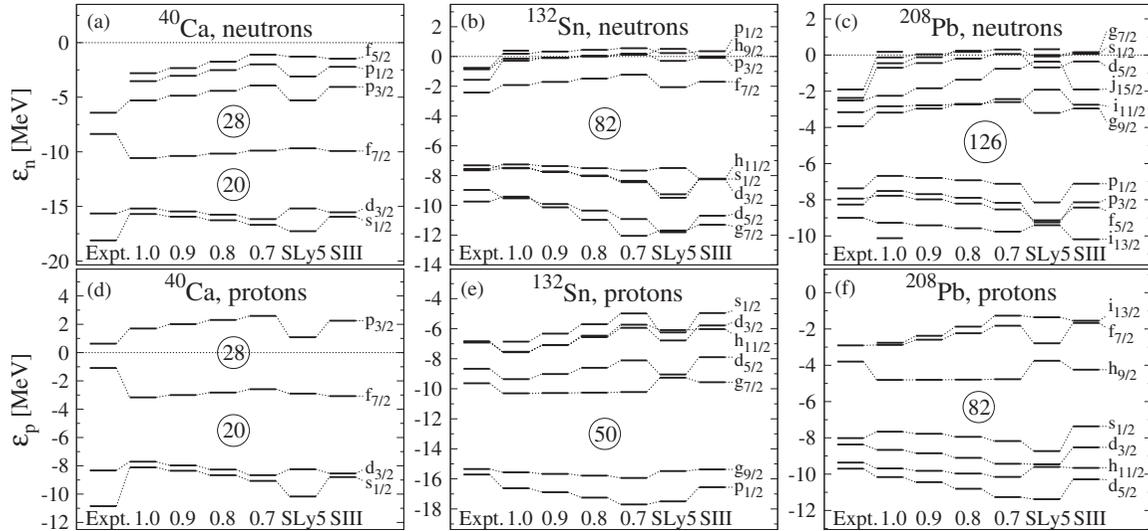
FIG. 7. Single-particle energies obtained as eigenvalues of the mean-field Hamiltonian in spherical calculations for ^{40}Ca (left), ^{132}Sn (center), and ^{208}Pb (right) for the parametrizations as indicated and compared with experimental data determined as one-nucleon separation energies to or from the doubly magic nucleus.

which correlations beyond the mean field can be expected to play a lesser role.

C. Deformed nuclei

In addition to the properties of singly magic nuclei, we also validate the performance of the new parametrizations for deformation and rotational properties of selected key nuclei.

1. Deformation energy curves

We start by studying nuclei that have been experimentally identified to be either deformed or have states of different deformation coexisting at low energy. In Fig. 8, the deformation energy curves of ^{24}Mg, ^{74}Kr, ^{80}Zr, ^{100}Zr, and ^{186}Pb are plotted as a function of the dimensionless axial quadrupole deformation

$$\beta_2 = \sqrt{\frac{5}{16\pi}} \frac{4\pi}{3R^2A} \langle 2z^2 - x^2 - y^2 \rangle, \qquad (8)$$

where $R = 1.2\,A^{1/3}$ fm. Experimentally, a prolate deformation for their ground state is well established for ^{24}Mg and ^{100}Zr. For ^{80}Zr, spectroscopic data suggest that the excited states of the ground state rotational band have a large quadrupole deformation with a β_2 value around 0.4. The sparse available data, however, do not rule out that the ground state of ^{80}Zr has a complicated structure that involves a large mixing of different deformations.

The only parametrization that gives rise to a pronounced prolate minimum for ^{24}Mg, ^{80}Zr, and ^{100}Zr is SIII. For both SLyIII.xx shown, the ground state of ^{80}Zr is spherical with a prolate minimum at a slightly higher energy, nearly degenerate with a very shallow oblate minimum, whereas the ground state of ^{100}Zr has a large prolate deformation, with an oblate minimum at smaller $|\beta_2|$ excited by around 1 MeV. For SLy5,

the ground state of ^{80}Zr is spherical with a prolate minimum excited by about 4 MeV. For ^{100}Zr, this parametrization gives nearly degenerate prolate and oblate minima. Before drawing conclusions on how well these topographies are compatible with experimental data, one has to estimate how the correlations that we plan to introduce explicitly in future applications might change the simple picture of energy curves. Rodríguez and Egido [74] have calculated the energy surface of ^{80}Zr, including triaxial quadrupole deformations using the Gogny force. They have found several spherical, axial, and triaxial minima. Before projection, the axial part of their energy surface is similar to the one obtained here with SLy5. For this nucleus, however, projection on angular momentum alters the topography of the energy surface, leading after configuration mixing to a ground state with a predominant component at a large quadrupole axial deformation.

A beyond-mean-field study of the neutron-deficient Kr isotopes using the Skyrme parametrization SLy6 has been published in Ref. [33]. After projection and mixing, the relative energy of prolate and oblate states leads to excitation spectra in disagreement with the experimental data. The energy curve obtained for ^{74}Kr with SLy5 resembles the one of SLy6 presented, such that it can be expected that SLy5 would also give similar results after configuration mixing. By contrast, the prolate minimum obtained with SIII and SLyIII.xx seems more realistic in view of the experimental data. Finally, the deformation energy curve of ^{186}Pb is alike for all parametrizations, displaying a spherical ground state and a prolate and oblate minimum within less than 1 MeV of excitation energy each.

It is remarkable that SIII and the SLyIII.xx parametrizations give a much more realistic description of the energy curves in the $A \approx 80$ region than the SLyx parametrizations. This difference, however, cannot be traced back directly to the linear density dependence, as some other Skyrme parametrizations with noninteger exponents α of the density dependence give
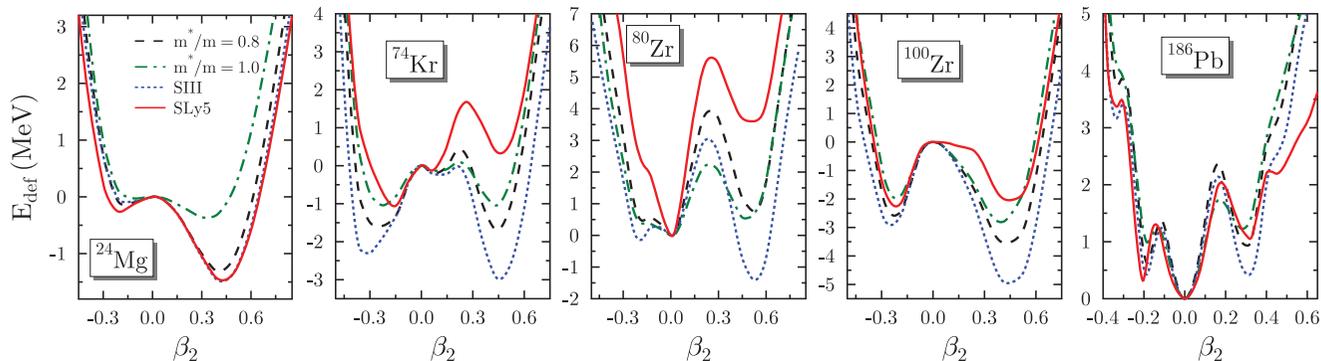
FIG. 8. (Color online) Potential energy curves along quadrupole deformation β_2 for ^{24}Mg, ^{74}Kr, ^{80}Zr, ^{100}Zr, and ^{186}Pb obtained by constraint HFB calculations.

an energy curve for ^{80}Zr that is much closer to the one of SIII than that of SLy5 [75].

The value of the effective mass has a clear effect on the variation of energy with deformation. Comparing the curves obtained with SLyIII.0.8 and SLyIII.1.0, one can see that a higher effective mass results in a flatter behavior of the deformation energy curves.

Overall, the SLyIII.*xx* parametrizations provide encouraging results for the deformation properties at the mean-field level. The following examples, however, will illustrate some limitations of these parametrizations.

2. Fission barrier of ^{240}Pu

In Fig. 9, the fission barrier of ^{240}Pu is presented as a function of quadrupole deformation. For all parametrizations, triaxiality was taken into account in the calculation of the first barrier and octupole deformations for the second barrier.

In all cases shown in the figure, the excitation energy of the fission isomer overestimates the experimental value, for which two conflicting values of $\sim$2.8 MeV [76] and 2.25 ± 0.20 MeV [77] can be found in the literature. In the same way, the energies of the inner and outer fission barriers overestimate the experimental values of 6.05 and 5.15 MeV, respectively
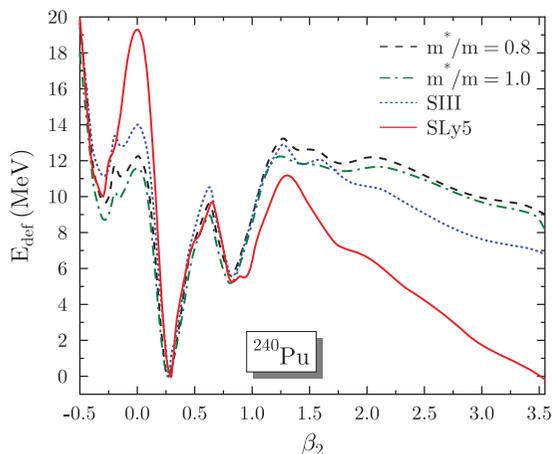
[78]. For SIII this deficiency long has been known [79]. Also, the results obtained with SLy5 are less realistic than those obtained with the SLy4 and SLy6 parametrizations discussed in Ref. [80]. However, one must take into account that the calculations performed in Ref. [80] and here are not fully equivalent: The pairing strength is not the same and the particle number projection was performed in Ref. [80] and is not used here. In that paper, it was shown that at the mean-field level, the energy of the fission isomer is close to the experimental value with SLy6, whereas SLy4 gives better agreement when beyond-mean-field correlations are taken into account. All parametrizations shown in Fig. 9 give energies for the fission isomer much larger than SLy4 when used with standard pairing, and beyond-mean-field correlations cannot be expected to be large enough to obtain agreement with the data for any of them.

The differences in barrier height for SIII and SLyIII.*xx* seen in Fig. 9 cannot be correlated with the value of the surface energy coefficient of these parametrizations. The values for SLy5 ($a_{\text{surf}} = 18.5$ MeV) and SIII (18.6 MeV) are very similar [81], whereas those for SLyIII.0.8 (19.5 MeV) and SLyIII.1.0 (19.4 MeV) are significantly larger. The value of the isoscalar effective mass, and thereby the average level density at the Fermi energy, does not play a crucial role either. However, the similarity of the energy curves obtained with SIII and all SLyIII.*xx* hints at an insufficiency of a simple linear density dependence to describe large deformation.

3. Superdeformed rotational band in ^{194}Hg

The next test of the new parametrizations concerns the description of superdeformed rotational bands (SD). These bands are well described all over the nuclear chart by self-consistent mean-field calculations and represent one of the most impressive successes of these approaches in the 1990s. The SD bands in the Hg region are of specific interest as the gradual increase of the dynamical moments of inertia $\mathcal{J}^{(2)}$,

$$\mathcal{J}^{(2)} = \frac{\partial \langle J_z \rangle}{\partial \omega} = \frac{1}{\omega} \frac{\partial \mathcal{E}}{\partial \omega}, \tag{9}$$

as a function of rotational frequency $\hbar\omega$ results from the gradual disappearance of pairing correlations and the alignment of the intruder orbitals. For further details we refer to our recent
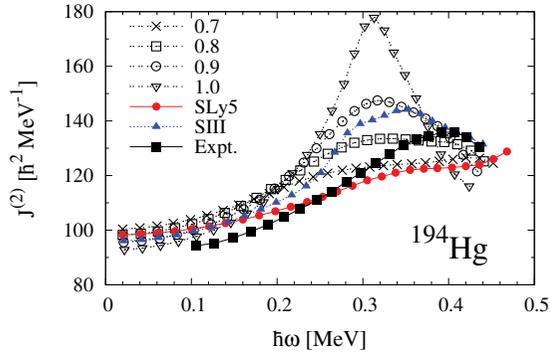

FIG. 9. (Color online) Fission barrier along quadrupole deformation β_2 for ^{240}Pu obtained by different Skyrme parameter sets.

FIG. 10. (Color online) Dynamical moment of inertia as a function of angular frequency $\hbar\omega$ for the superdeformed rotational band in ^{194}Hg obtained with the parametrizations as indicated.

detailed analysis of the various contributions of the EDF to $\mathcal{J}^{(2)}$ in Ref. [55]. The dynamical moments of inertia for the ground SD band of ^{194}Hg are presented in Fig. 10. For SIII and SLyIII.*xx*, the peak in the $\mathcal{J}^{(2)}$ appears at too low an $\hbar\omega$ and, overall, the description of the experimental data is less satisfactory than that of other Skyrme parametrizations such as SLy4 or SkM*. It should be noted that the currently used pairing strength V_0 is rather low in comparison with the typical values of $V_0 = -1250$ MeV fm^3 that was determined in SD bands. An increase of the pairing strength, however, will have very little influence on the location of the peak in $\mathcal{J}^{(2)}$.

4. Single-particle levels in deformed transactinide nuclei

Previous studies of odd-mass transactinides [82] have put into evidence some major drawbacks in the spectra obtained with the current Skyrme parametrizations. We have tested the parametrizations that we have constructed in this work on two nuclei, ^{251}Cf and ^{249}Bk, for which very detailed data are available and which have been studied in Ref. [82]. The same method as in Ref. [82] has been used. Each state results from a self-consistent calculation of a one-quasiparticle excitation on an even-even HFB vacuum. In this way, the polarization effect due to the quasiparticle excitation and the terms in the Skyrme EDF depending on time-odd densities are taken into account self-consistently. The results are shown in Fig. 11. The ^{251}Cf spectra exhibit the expected effect of the effective mass: The spectrum becomes more dense when the effective mass is increased. Note, however, that the compression of the spectrum is not uniform and that the changes do not correspond to a simple scaling proportional to the ratios of effective masses as it is sometimes assumed [85]. Moreover, the order of the levels can differ when comparing the parametrizations. The nontrivial effective mass dependence is still more apparent for the spectrum of ^{249}Bk, where the first excited state is lower in energy for the lowest values of the effective mass and does not have the same quantum numbers for all the parametrizations. Although the obtained spectra depend on the parametrizations, none of the SLyIII.*xx* corrects the main drawbacks of previous EDF parametrizations, i.e., the misplacement of some levels that may be connected with specific spherical single-particle orbitals.
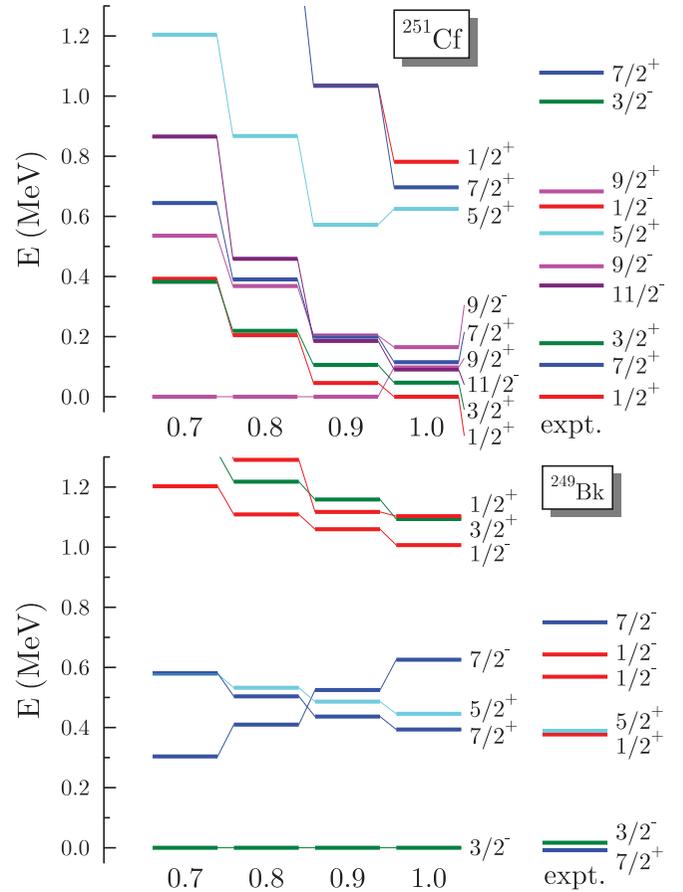

FIG. 11. (Color online) Low-lying one-quasiparticle states in ^{251}Cf and ^{249}Bk. Experimental data are taken from Refs. [83,84].

5. Particle number symmetry restored deformation energy surfaces

The main motivation of the present study was to construct a Skyrme functional that can be used in regularized MR EDF calculations. In Fig. 12, we show, as an example of such a calculation, the particle-number restored deformation energy surfaces of ^{24}Mg without and with regularization in one sextant of the β-γ plane. The calculations were performed as described in Ref. [49] with two differences. The first one is the use of SLyIII.0.8, and the second one is the use of the extension of the regularization scheme to trilinear terms in the same particle species as is required by this parametrization. We use Fomenko's prescription [49] with 19 discretization points for the gauge-space integrals. At small deformation, the difference between the regularized and nonregularized energy surfaces is quite dramatic. Without regularization, the absolute minimum is located in a region where the spurious contribution to the EDF is particular large. It is only with the regularization that one finds the usual topography of the energy surface with a prolate axial minimum.

The nature and size of problems with spurious contributions to the MR EDF depend strongly on the parametrization of the functional. The presence of terms that are trilinear in the same particle species in SLyIII.0.8 makes the deformation and discretization dependence of the spurious energies much
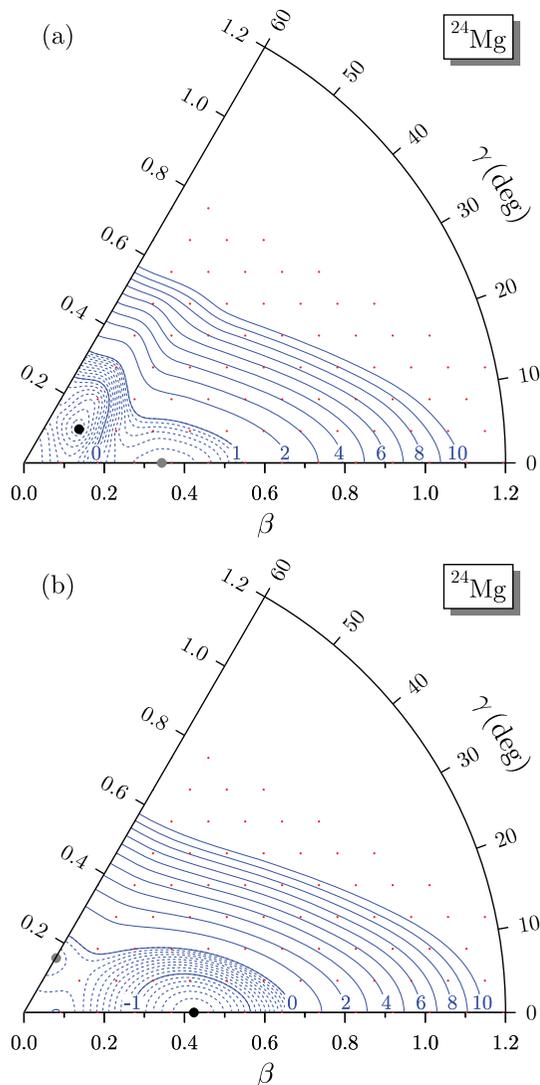
FIG. 12. (Color online) Particle-number restored deformation energy surface of ^{24}Mg in the β-γ plane constructed with the SLyIII.0.8 MR EDF without (a) and with regularization (b) of the MR EDF. Solid black circles indicate the location of the absolute minimum of each energy surface and gray circles the location of secondary minima. The dots indicate the calculated points.

more violent than what is found for the SIII parametrization used in the regularized calculations Ref. [49]. Also, there are no evident problems in the (nonregularized) particle-number projected energy surfaces of ^{24}Mg obtained with SLy4 and presented in Ref. [34]. There we encountered obvious irregularities only when projecting simultaneously on particle number and angular momenta $J > 0$.

A detailed discussion of the regularization that will also address its application to angular-momentum projection and general configuration mixing will be given elsewhere [86].

IV. SUMMARY

The present study is a part of our program to construct an effective interaction of high spectroscopic quality for mean-field and beyond-mean-field calculations. In this first step, we have constructed a regularizable (in the sense of Ref. [43]) EDF within the standard form of the Skyrme EDF. This requires that the power α of the density dependence takes an integer value. The simple form of the non-momentum-dependent trilinear terms used here has known deficiencies. It forbids us to obtain a value for the incompressibility compatible with the empirical value. We have shown also the problems encountered in the description of charge radii, fission barriers heights, and moments of inertia in SD bands in the $A \approx 190$ region. However, the protocol that we have developed leads to a significantly improved description of shape coexistence in the $A \approx 80$ region.

The four variants with different isoscalar effective mass will enable studies on how the correlation energy in beyond-mean-field methods depends on the effective mass. However, the mean-field results presented here show a clear preference for $m_0^*/m = 0.8$.

Even with their deficiencies, the present parametrizations will allow us to analyze and benchmark the performance of the regularization. Work in that direction is underway [86].

Higher-order terms (i.e., at least trilinear terms with derivatives) are clearly necessary to remove the deficiencies of the SLyIII.xx parametrizations pinpointed here and to improve the predictive power of regularizable Skyrme-type functionals. Work in that direction is also underway [50,51]. Alternative (non-Skyrme-type) regularizable forms of the density dependence might be considered as well, as, for example, the form proposed in Ref. [87]. The moment a form of a sufficiently flexible functional that is safely usable in MR EDF calculations has been established, fits should be performed on the level of MR EDF.

[1] M. Bender, P.-H. Heenen, and P.-G. Reinhard, Rev. Mod. Phys. **75**, 121 (2003).

[2] T. H. R. Skyrme, Philos. Mag. **1**, 1043 (1956).

[3] T. H. R. Skyrme, Nucl. Phys. **9**, 615 (1958).

[4] D. Vautherin and D. M. Brink, Phys. Rev. C **5**, 626 (1972).

[5] D. Vautherin, Phys. Rev. C **7**, 296 (1973).

[6] M. Beiner, H. Flocard, Nguyen Van Giai, and P. Quentin, Nucl. Phys. A **238**, 29 (1975).

[7] J.-P. Blaizot, D. Gogny, and B. Grammaticos, Nucl. Phys. A **265**, 315 (1976).

[8] J.-P. Blaizot, Phys. Rep. **64**, 171 (1980).

[9] G. Colò, N. V. Giai, J. Meyer, K. Bennaceur, and P. Bonche, Phys. Rev. C **70**, 024307 (2004).

[10] B. D. Chang, Phys. Lett. B **56**, 205 (1975).

[11] S. O. Bäckman, A. D. Jackson, and J. Speth, Phys. Lett. B **56**, 209 (1975).

[12] M. Waroquier, K. Heyde, and H. Vinckx, Phys. Rev. C **13**, 1664 (1976).

[13] S. Stringari, R. Leonardi, and D. M. Brink, Nucl. Phys. A **269**, 87 (1976).

[14] J. P. Blaizot, Phys. Lett. B **60**, 435 (1976).

[15] M. Beiner and R. J. Lombard, Ann. Phys. **86**, 262 (1974).

[16] H. Krivine, J. Treiner, and O. Bohigas, Nucl. Phys. A **336**, 155 (1980).

[17] H. A. Bethe, Annu. Rev. Nucl. Sci. **21**, 93 (1971).

[18] H. S. Köhler and Y. C. Lin, Nucl. Phys. A **136**, 35 (1969).

[19] H. S. Köhler, Phys. Rep. **18**, 217 (1975).

[20] H. S. Köhler, Nucl. Phys. A **258**, 301 (1976).

[21] D. Gogny, in *Proceedings of the International Conference on Nuclear Self-Consistent Fields, International Centre for Theoretical Physics, Trieste*, edited by G. Ripka and M. Porneuf (North-Holland, Amsterdam, 1975), p. 333.

[22] J. Dechargé and D. Gogny, Phys. Rev. C **21**, 1568 (1980).

[23] E. Chabanat, P. Bonche, P. Haensel, J. Meyer, and R. Schaeffer, Nucl. Phys. A **627**, 710 (1997).

[24] E. Chabanat, P. Bonche, P. Haensel, J. Meyer, and R. Schaeffer, Nucl. Phys. A **635**, 231 (1998).

[25] P. Fleischer, P. Klüpfel, P.-G. Reinhard, and J. A. Maruhn, Phys. Rev. C **70**, 054321 (2004).

[26] L. Prochniak, P. Quentin, D. Samsœn, and J. Libert, Nucl. Phys. A **730**, 59 (2004).

[27] P.-H. Heenen, P. Bonche, J. Dobaczewski, and H. Flocard, Nucl. Phys. A **561**, 367 (1993).

[28] H. Zduńczuk, W. Satuła, J. Dobaczewski, and M. Kosmulski, Phys. Rev. C **76**, 044304 (2007).

[29] M. Bender, G. F. Bertsch, and P.-H. Heenen, Phys. Rev. C **73**, 034322 (2006).

[30] H. Flocard and D. Vautherin, Nucl. Phys. A **264**, 197 (1976).

[31] P. Bonche, J. Dobaczewski, H. Flocard, P.-H. Heenen, and J. Meyer, Nucl. Phys. A **510**, 466 (1990).

[32] N. Tajima, H. Flocard, P. Bonche, J. Dobaczewski, and P.-H. Heenen, Nucl. Phys. A **542**, 355 (1992).

[33] M. Bender, P. Bonche, and P.-H. Heenen, Phys. Rev. C **74**, 024312 (2006).

[34] M. Bender and P.-H. Heenen, Phys. Rev. C **78**, 024309 (2008).

[35] T. Lesinski, M. Bender, K. Bennaceur, T. Duguet, and J. Meyer, Phys. Rev. C **76**, 014312 (2007).

[36] M. Bender, K. Bennaceur, T. Duguet, P.-H. Heenen, T. Lesinski, and J. Meyer, Phys. Rev. C **80**, 064302 (2009).

[37] M. Kortelainen, J. Dobaczewski, K. Mizuyama, and J. Toivanen, Phys. Rev. C **77**, 064307 (2008).

[38] R. Balian and E. Brezin, Nuovo Cim. B **64**, 37 (1969).

[39] R. Rodríguez-Guzmán, J. L. Egido, and L. M. Robledo, Nucl. Phys. A **709**, 201 (2002).

[40] J. M. Yao, J. Meng, P. Ring, and D. Vretenar, Phys. Rev. C **81**, 044311 (2010).

[41] M. Anguiano, J. L. Egido, and L. M. Robledo, Nucl. Phys. A **696**, 467 (2001).

[42] J. Dobaczewski, M. V. Stoitsov, W. Nazarewicz, and P. G. Reinhard, Phys. Rev. C **76**, 054315 (2007).

[43] D. Lacroix, T. Duguet, and M. Bender, Phys. Rev. C **79**, 044318 (2009).

[44] T. Duguet, M. Bender, K. Bennaceur, D. Lacroix, and T. Lesinski, Phys. Rev. C **79**, 044320 (2009).

[45] J. L. Egido and L. M. Robledo, Nucl. Phys. A **524**, 65 (1991).

[46] T. Duguet and P. Bonche, Phys. Rev. C **67**, 054308 (2003).

[47] L. M. Robledo, Int. J. Mod. Phys. E **16**, 337 (2007).

[48] L. M. Robledo, J. Phys. G **37**, 064020 (2010).

[49] M. Bender, T. Duguet, and D. Lacroix, Phys. Rev. C **79**, 044319 (2009).

[50] J. Sadoudi, Ph.D. thesis, Université Paris-Sud XI, 2011.

[51] J. Sadoudi, K. Bennaceur, T. Duguet, J. Meyer *et al.* (to be published).

[52] M. Kortelainen, T. Lesinski, J. More, W. Nazarewicz, J. Sarich, N. Schunck, M. V. Stoitsov, and S. Wild, Phys. Rev C **82**, 024313 (2010).

[53] M. Kortelainen, J. McDonnell, W. Nazarewicz, P.-G. Reinhard, J. Sarich, N. Schunck, M. V. Stoitsov, and S. M. Wild, Phys. Rev C **85**, 024304 (2012).

[54] E. Engel and R. M. Dreizler, *Density Functional Theory* (Springer, New York, 2011).

[55] V. Hellemans, P.-H. Heenen, and M. Bender, Phys. Rev. C **85**, 014326 (2012).

[56] J. Terasaki, P.-H. Heenen, P. Bonche, J. Dobaczewski, and H. Flocard, Nucl. Phys. A **593**, 1 (1995).

[57] S. J. Krieger, P. Bonche, H. Flocard, P. Quentin, and M. S. Weiss, Nucl. Phys. A **517**, 275 (1990).

[58] B. A. Brown, Phys. Rev. C **58**, 220 (1998).

[59] B. A. Brown, W. A. Richter, and R. Lindsay, Phys. Lett. B **483**, 49 (2000).

[60] S. Goriely and J. M. Pearson, Phys. Rev. C **77**, 031301(R) (2008).

[61] M. Bender, K. Rutz, P.-G. Reinhard, and J. A. Maruhn, Eur. Phys. J. A **7**, 467 (2000).

[62] R. B. Wiringa, V. Fiks, and A. Fabrocini, Phys. Rev. C **38**, 1010 (1988).

[63] T. Lesinski, K. Bennaceur, T. Duguet, and J. Meyer, Phys. Rev. C **74**, 044315 (2006).

[64] G. Audi, A. H. Wapstra, and C. Thibault, Nucl. Phys. A **729**, 337 (2003).

[65] E. G. Nadjakov, K. P. Marinova, and Y. P. Gangrsky, At. Data Nucl. Data Tables **56**, 133 (1994).

[66] F. Le Blanc *et al.*, Phys. Rev. C **72**, 034305 (2005).

[67] M. Bender, K. Rutz, P.-G. Reinhard, and J. A. Maruhn, Eur. Phys. J. A **8**, 59 (2000).

[68] M. Yamagami, Y. R. Shimizu, and T. Nakatsukasa, Phys. Rev. C **80**, 064301 (2009).

[69] http://orph02.phy.ornl.gov/workshops/lacm08/UNEDF/DataSet04.dat

[70] T. Duguet and G. Hagen, Phys. Rev. C **85**, 034330 (2012), and references therein.

[71] E. Litvinova and P. Ring, Phys. Rev. C **73**, 044328 (2006).

[72] G. Colò, H. Sagawa, and P. F. Bortignon, Phys. Rev. C **82**, 064307 (2010).

[73] M. Bender, G. F. Bertsch, and P.-H. Heenen, Phys. Rev. C **78**, 054312 (2008).

[74] T. R. Rodriguez and J. L. Egido, Phys. Lett. B **705**, 255 (2011).

[75] P.-G. Reinhard, D. J. Dean, W. Nazarewicz, J. Dobaczewski, J. A. Maruhn, and M. R. Strayer, Phys. Rev. C **60**, 014316 (1999).

[76] B. Singh, R. Zywina, and R. B. Firestone, Nucl. Data Sheets **97**, 241 (2002).

[77] M. Hunyadi, D. Gassmann, A. Krasznahorkay, D. Habs, P. G. Thirolf, M. Csatlós, Y. Eisermann, T. Faestermann, G. Graw, J. Gulyas, R. Hertenberger, H. J. Maier, Z. Mátáa, A. Metz, and M. J. Chromik, Phys. Lett. B **505**, 27 (2001).

[78] R. Capote, M. Herman, P. Obložinský, P. G. Young, S. Goriely, T. Belgya, A. V. Ignatyuk, A. J. Koning, S. Hilaire, V. A. Plujko, M. Avrigeanu, O. Bersillon, M. B. Chadwick, T. Fukahori, Zhigang Ge, Yinlu Han, S. Kailas, J. Kopecky, V. M. Maslov, G. Reffo, M. Sin, E. Sh. Soukhovitskii, and P. Talou, Nucl. Data Sheets **110**, 3107 (2009); Reference Input Parameter Library (RIPL-3) http://www-nds.iaea.org/RIPL-3/.

[79] J. Bartel, P. Quentin, M. Brack, C. Guet, and H.-B. Håkansson, Nucl. Phys. A **386**, 79 (1982).

[80] M. Bender, P.-H. Heenen, and P. Bonche, Phys. Rev. C **70**, 054304 (2004).

[81] R. Jodon, K. Bennaceur, M. Bender, and J. Meyer (to be published).

[82] M. Bender, P. Bonche, T. Duguet, and P.-H. Heenen, Nucl. Phys. A **723**, 354 (2003).

[83] A. Artna-Cohen, Nucl. Data Sheets **88**, 155 (1999).

[84] I. Ahmad, M. P. Carpenter, R. R. Chasman, J. P. Greene, R. V. F. Janssens, T. L. Khoo, F. G. Kondev, T. Lauritsen, C. J. Lister, P. Reiter, D. Seweryniak, A. Sonzogni, J. Uusitalo, I. Wiedenhöver, and P. Bhattacharyya, Phys. Rev. C **62**, 064302 (2000).

[85] A. V. Afanasjev and S. Shawaqfeh, Phys. Lett. B **706**, 177 (2011).

[86] M. Bender, B. Avez, B. Bally, T. Duguet, P.-H. Heenen, and D. Lacroix (to be published).

[87] A. Gezerlis and G. F. Bertsch, Phys. Rev. Lett. **105**, 212501 (2010).